Modelling of Work-Hardening during Hot Rolling of V and Nb Microalloyed Steels in the Low Austenite Temperature Region

Chalimba S.A.J., Mostert R.J., Stumpf W.E., Siyasiya C.W., Banks K.M.
Department of Materials Science and Metallurgical Engineering, University of Pretoria, Hatfield, Pretoria, Republic of South Africa
Corresponding author: Tel: +27 606 033 216
Email: stephenchalimba@yahoo.com

Key words: dynamic recovery, dynamic recrystallization, dynamic transformation, hot rolling, modelling, work hardening

Abstract

This work extends the application of the well-established Estrin and Mecking (EM) work-hardening model in work hardened or unstable austenite deformed in the lower austenite temperature region. It considers the interaction between work hardening, dynamic recovery and dynamic softening attributed to dynamic recrystallization and dynamic transformation to ferrite. Experimental parameters were varied to study the effects of strain, strain rate and temperature on hot working behaviour during hot rolling in this austenite at temperatures in the lower austenite region. Hot compression tests were performed on two V and Nb microalloyed steels respectively, at strain rates between 0.1 and 10 s^{-1} over a temperature range of 750 to 1000 ^oC. A model is presented describing the influence of dynamic recovery on flow behaviour, applicable to the unstable austenite phase region. The modified work-hardening model incorporates an additional fitting parameter to the EM model and is dependent on the recovery and softening rates. The new model improved prediction in the unstable austenite region, whilst the original EM model gave better correlation at relatively higher temperatures when Dynamic Recrystallization (DRX) is dominant or at relatively lower temperatures when only Dynamic Recrystallization (DT) to ferrite was the softening mechanism.

1.0 Introduction

Understanding the strain-hardening of metals is one of the most important fields of research in physical metallurgy [1]. Most work on the hot rolling behaviour of VN steels has been on medium carbon low alloy vanadium steels with a focus on the stable austenite temperature range (between 950-1150 ^oC) and at quasi-static strain rates of 0.001 to 0.1 s^{-1} [2, 3, 4]. In these studies, dynamic recrystallization (DRX) was considered as the dominant softening mechanism due to the low stacking fault energy (SFE) of the stable austenite and the relatively low strain rates used [4, 5]. This work, therefore, focuses on studying the hot rolling behaviour of VN microalloyed steels in the unstable austenite temperature region (between 750-1000 ^oC) at moderate strain rates (between 0.1 and 10 s^{-1}). The hot workability of the VN microalloyed steel was assessed in comparison to that of a reference Nb-Ti microalloyed steel.

Kocks and Mecking, and Estrin and Mecking, respectively proposed phenomenological models for the macroscopic plasticity of metals to describe the plastic flow during continuous deformation and athermal work-hardening, respectively [6]. The application of both the Kocks and Mecking (KM) and the Estrin and Mecking (EM) models are limited to stage 2 and 3 of strain hardening but extensions to the model, which generally include softening due to dynamic recrystallization, allow application of the model in stage 4 and 5 (no strain hardening) [1, 6]. The KM and EM models use two internal variables to describe either dislocations in cells or dislocations in walls [1]. Bouaziz [1] noted that, although both models use a linear relationship between the annihilation term by dynamic recovery and the dislocation density, the number of fitting parameters should increase.

In this study, a modified DRV work-hardening model was formulated with an additional fitting parameter applicable to the DRX/DT inter-mode region, i.e. the unstable austenite region. The model considers a linear relationship between an annihilation term by recovery and dynamic transformation, and the dislocation density.

2.0 Experimental Method

2.1 Composition and sample preparation

VN and Nb-Ti microalloyed steels with chemical compositions given in Table I, were studied. For the VN steel, a vacuum induction melted ingot was hot rolled to 13 mm diameter bar, whilst the Nb-Ti steel specimens were wire cut from an as-cast industrial slab. Axisymmetric hot compression specimens were wire cut to a height of 15 mm and diameter of 10 mm whereas dilatometric samples were machined to a height of 10 mm and diameter of 5 mm.

Table I – Chemical composition (mass-%) for the steels investigated

Steel	**Element**								
	C	**Mn**	**Si**	**Al**	**Nb**	**Ti**	**V**	**N**	**Fe**
VN	0.06	1.69	0.29	0.049	0.0015	Trace	0.062	0.0097	Bal.
Nb-Ti	0.09	0.88	0.20	0.043	0.025	0.017	0	0.0088	Bal.

Note: Combustiometric chemical analysis was used in the determination of C and N

2.2 Mechanical testing

Gleeble^{TM} 1500 and Gleeble^{TM} 3500 series thermomechanical simulators fitted with tungsten carbide anvils were used for isothermal uniaxial axisymmetric compression tests. The platens were lubricated either with tantalum foil or graphite and nickel paste.

The specimens were deformed in accordance with the schematic schedule shown in

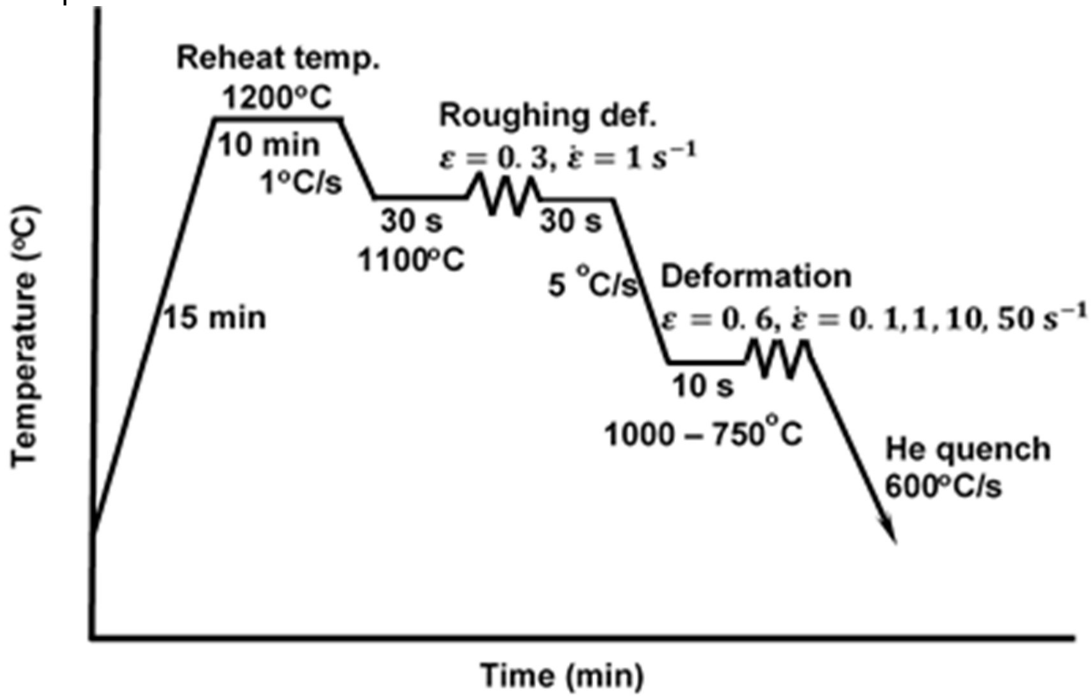

Figure 1 [7]. An austenitisation temperature of 1200 °C was applied in all tests based on typical industrial practice and dissolution temperatures of both V(C,N) – 854 °C and Nb(C,N) – 1092 °C were determined from ThermoCalc® 4.1 property diagrams using the TCFE7 database. The criteria used for the validity of the hot compression tests during upsetting was assumed when the test validity criteria for each experiment as outlined in Ref. [8, 9, 10] was met. The testing criteria included: the aspect ratio, and barrelling, height, ovality and circularity coefficients.

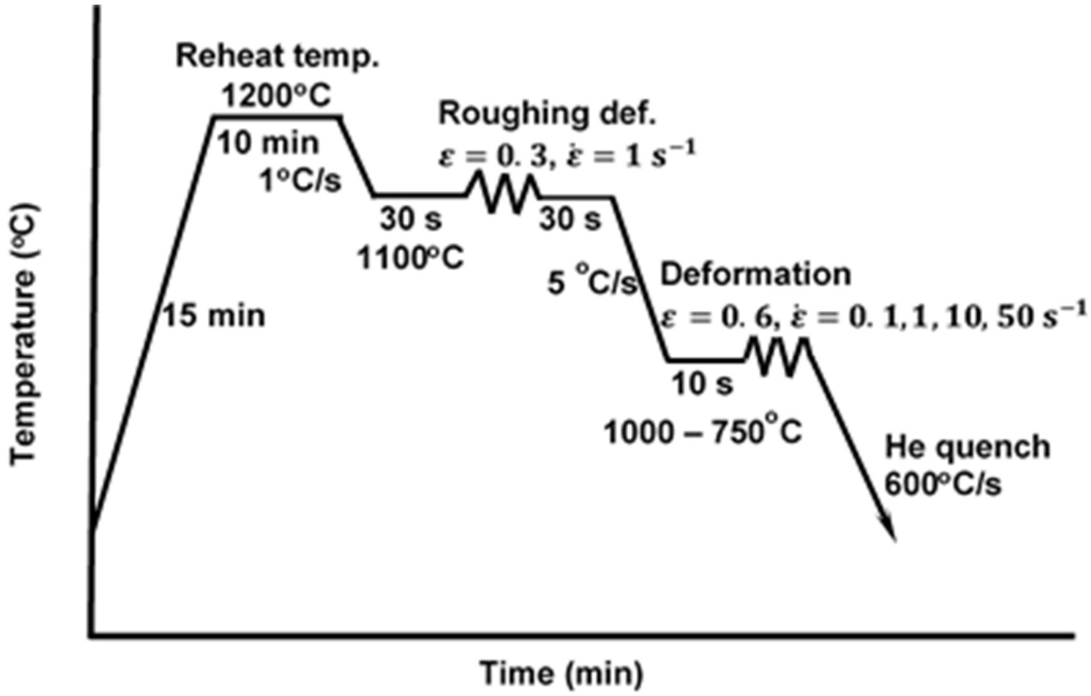

Figure 1 – Schematic representation of deformation test schedules. True strain and strain rate are represented as ε and $\dot{\varepsilon}$, respectively.

The Ar3 temperatures after the first hit in

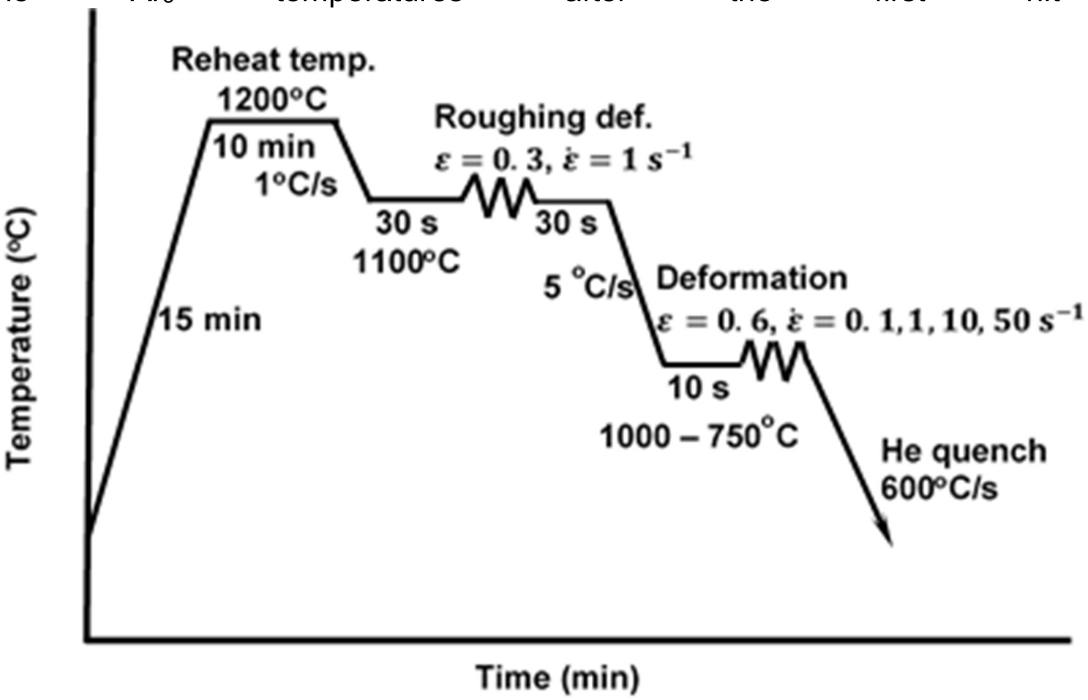

Figure 1 was determined to be 843 °C for the VN steel and 818 °C for the Nb-Ti steel at a cooling rate of 5 °C/s, see Ref. [7]. The dilatation curves in Ref. [7] were used to determine the ferrite volume fractions at the start of the final deformation step.

2.3 Post-deformation flow stress data processing

A detailed flow curve analysis included the use of central differences, whilst graphical methods involved polynomial fitting and regression analysis of flow stress-strain data. Care was taken not to mask any metallurgical phenomena on the flow data. The curves were fitted to the work-hardening flow curve using the yield stress σ_0 which was determined using the 2 % offset strain method. The plastic flow curve segment was fitted and smoothed with a 6th order polynomial using the Excel^{TM} software. The percentage error attributable to the error inherent in temperature, load measurement, lubrication breakdown and non-uniform flow was expected to be below 4% [11].

An assessment of theoretical modelling of the flow behaviour was performed up to the saturation stress (σ_{sat}) considering only work hardening and DRV. The study considered the favoured approaches commonly used – the MK and EM approaches (see Appendix 1 – Derivation of the Estrin and Mecking work hardening model) [12]. The MK approach uses linear sections of the $\theta - \sigma$ plots. The EM model uses the linearity of $\sigma\theta - \sigma^2$ plots to define the DRV (including recovery factor) and DT regimes. The deviation from linearity signified the critical stress, $\sigma_{c\ DRX}$.

3.0 Results

3.1 Flow curve behaviour

Figure **2** a) to f) shows the flow stress curves for both VN and Nb-Ti steel specimens deformed to an equivalent true strain of 0.6, at temperatures between 750 to 1000 °C and strain rates between 0.1 and 10 s^{-1} as per the deformation schedule given in

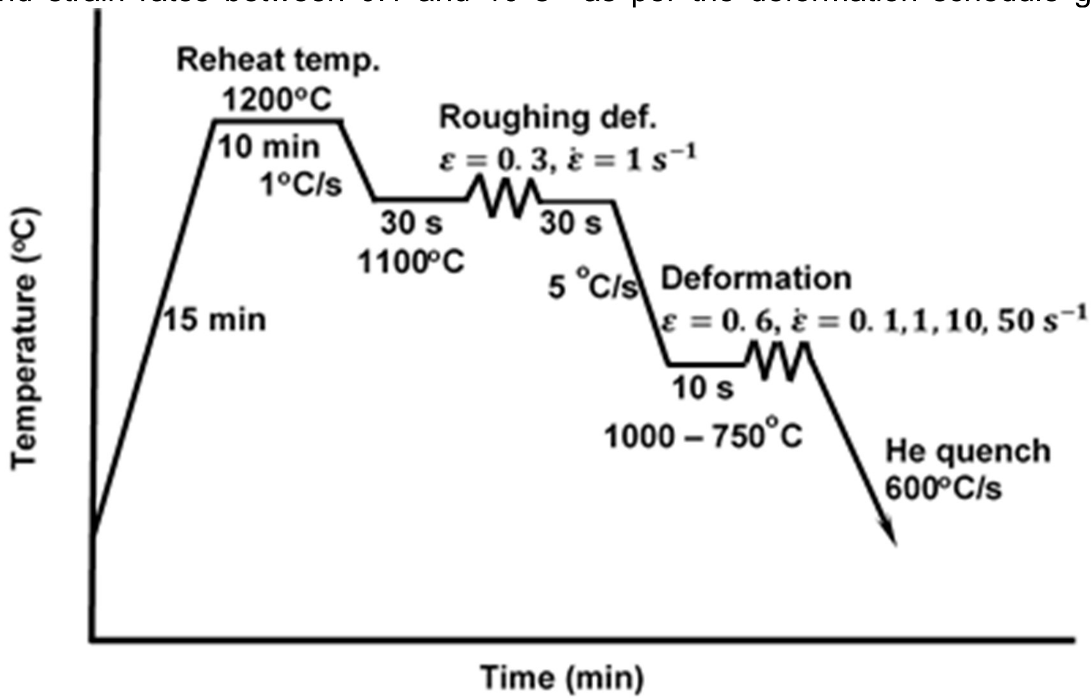

Figure 1. At low strain rates, the curves corresponding to deformation temperatures higher than 950 °C exhibit typical DRX behaviour with a single peak stress followed by a gradual fall towards a steady state stress. The peak stress becomes less obvious when the strain rate is increased and/or the deformation temperature is decreased. A 2% offset strain was used to distinguish the linear portion from the plastic flow curve as it coincided with the end of yield stress stagnation in most flow curves. The yield stress ($\sigma_{0.02}$) and equivalent strain ($\varepsilon_{0.02}$) are given in Table II and Table III for the VN and Nb-Ti steels, respectively.

The increase in stress levels with decreasing temperature was erratic in the Nb-Ti steel compared to the VN steel at 10 s^{-1} strain rate, whilst the reverse was true at 0.1 s^{-1} strain rate. The fluctuations in flow stress at high strain rates corresponded to the typical mill load fluctuations experienced during hot rolling of Nb-Ti steels compared to the gradual flow stress increases experienced in the deformation of VN steels.

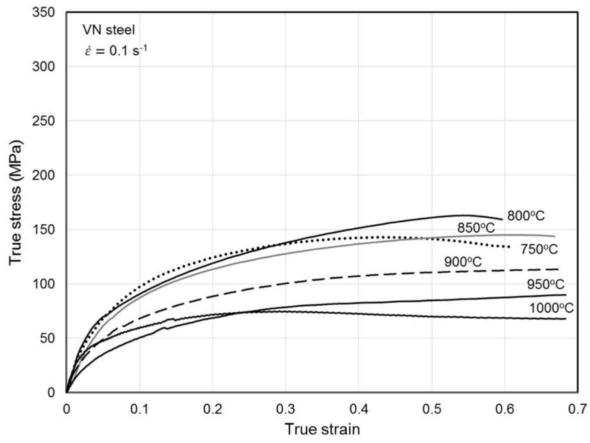

a) VN flow curves at a strain rate of 0.1 s^{-1}

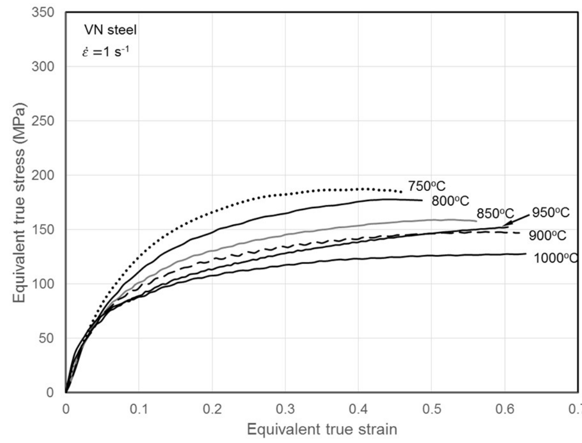

b) VN flow curves at a strain rate of 1 s^{-1}

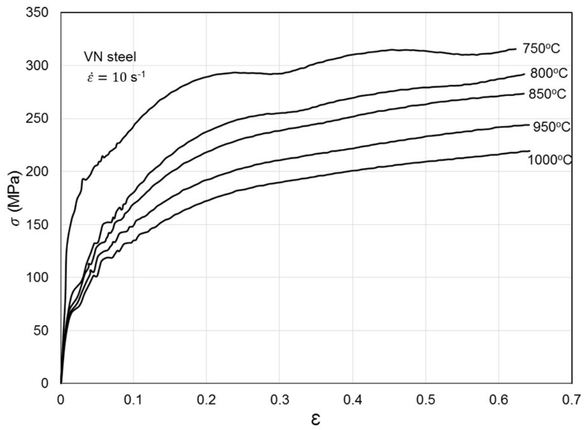

c) VN flow curves at a strain rate of 10 s^{-1}

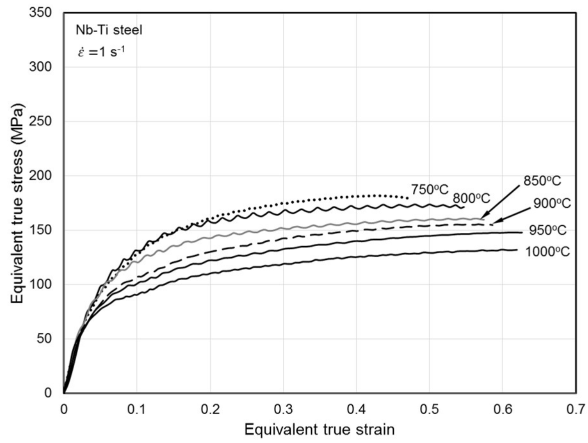

e) Nb-Ti steel flow curves at a strain rate of 1 s^{-1}

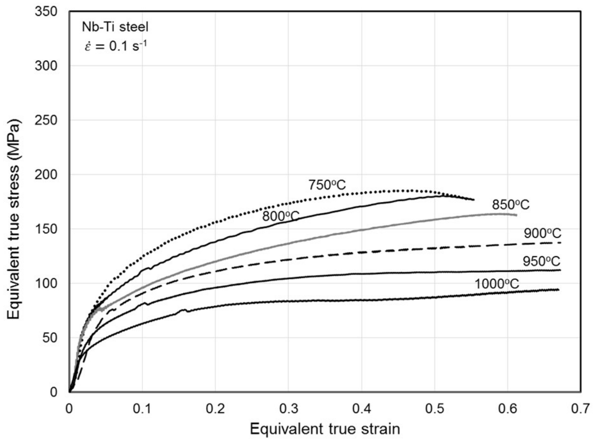

d) Nb-Ti steel flow curves at a strain rate of 0.1 s^{-1}

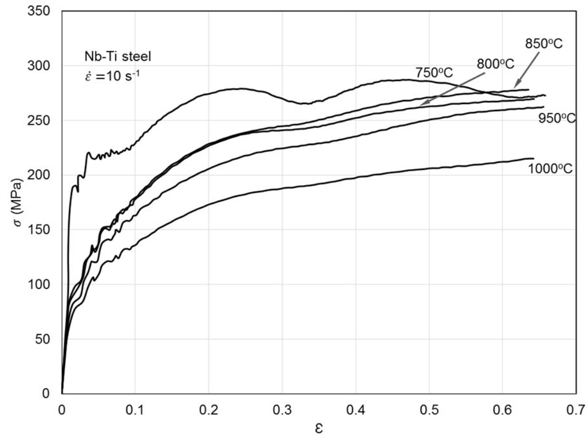

f) Nb-Ti steel flow curves at a strain rate of 10 s^{-1}

Figure 2 – Flow curves for the VN steel a) to c) and the Nb-Ti steel d) to f) at strain rates of 0.1, 1 and 10 s^{-1}

3.2 The Kocks and Mecking approach (KM model)

The work hardening-stress or $\theta - \sigma$ plots at different temperatures (750 – 1000 °C) and strain rates (0.1 – 10 s^{-1}) are given in Figure **3** a) – c) for the VN steel and Figure **3** d) – f) for the Nb-Ti steel respectively. Generally, the $\theta - \sigma$ plots in Figure **3** had either a single linear decrease or an initial linear decrease which was followed by a lower gradient linear section before the drop towards $\theta = 0$ at peak stress. Although in many studies the second linear segment signifies the start and end respectively of subgrain formation, referred to as the dynamic recovery (DRV) regime, in this study the second segment was found to coincide with the start of dynamic transformation ($\sigma_{c\ DT}$) from austenite to ferrite, see Figure **3** a). In agreement with other studies, the first and second abscissas of the $\theta - \sigma$ curve (i.e. intercepts at $\theta = 0$) signified the peak stress σ_p and the steady state stress σ_{ss} respectively, and are given in Table **II** for the VN steels and **Table III** for the Nb-Ti steels. The $\sigma_{c\ DRX}$ is given by the inflection point from linearity in the $\theta - \sigma$ curves which is also mathematically given by the global minima in $-d\theta/d\sigma$ versus σ curves or the abscissa in plots of $-d^2\theta/d\sigma^2$ versus σ ($\sigma_{c\ DRX}$ signifies the nucleation start for DRX grains), see Figure **3** a).

3.2.1 Critical stresses for VN steel

*Strain rate of 0.1 s^{-1}, **Figure 3** a):* Some partial DT for deformation at temperatures between 750 and 900 °C was found. As expected, an increase in peak stress with a decrease in temperature (thermal work hardening) was observed except at 750 °C where the peak stress was lower than that obtained at 800 and 850 °C.

*Strain rate of 1 s^{-1}, **Figure 3** b):* The peak stress was only attained at temperatures ranging from 750 to 900 °C. Minimal DRV was noticeable at temperatures between 800 and 950 °C. No steady state conditions were attained at all temperatures for deformation at a strain rate of 1 s^{-1}.

Strain rate of 10 s^{-1}, Figure 3 c): Partial DRX was present at 950 °C and above while partial DT was dominant at temperatures lower than 950 °C.

3.2.2 Critical stresses for Nb-Ti steel

Strain rate of 0.1 s^{-1}, Figure 3 d): A peak stress was reached for deformation at 850 to 750 °C and the linear relationship before σ_c was lost for all $\theta - \sigma$ curves.

Strain rate of 1 s^{-1}, Figure 3 e): The linear sections in the wavy $\theta - \sigma$ curves showed partial DT taking place at all temperatures and the peak was attained at temperatures below 950 °C. The peak stress increased gradually with a decrease in temperature.

Strain rate of 10 s^{-1}, Figure 3 f): Cyclic or non-monotonic work hardening was observed and a peak was not attained at all temperatures, however, partial DT and DRX was present.

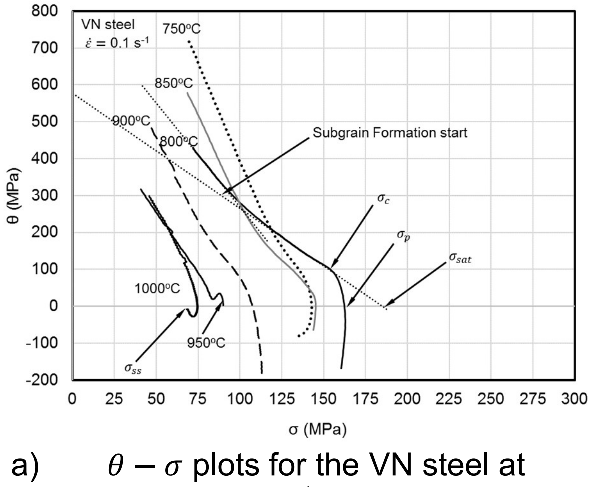

a) $\theta - \sigma$ plots for the VN steel at 0.1 s^{-1}

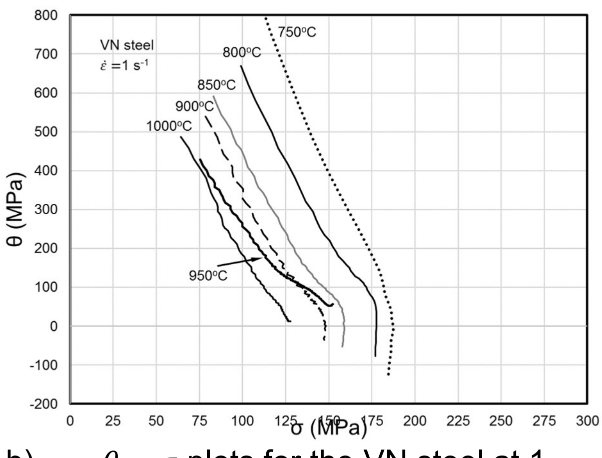

b) $\theta - \sigma$ plots for the VN steel at 1 s^{-1}

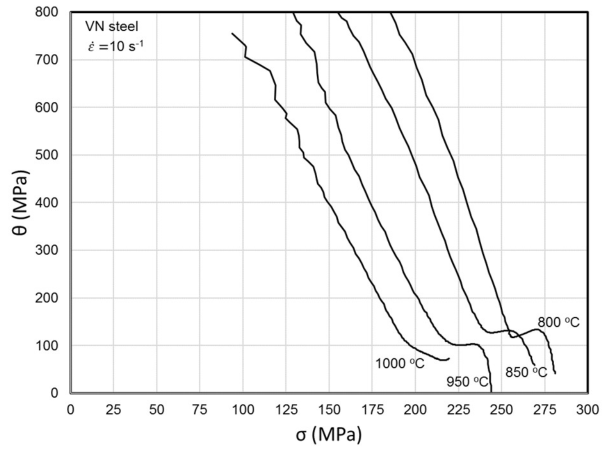

c) $\theta - \sigma$ plots for the VN steel at 10 s-1

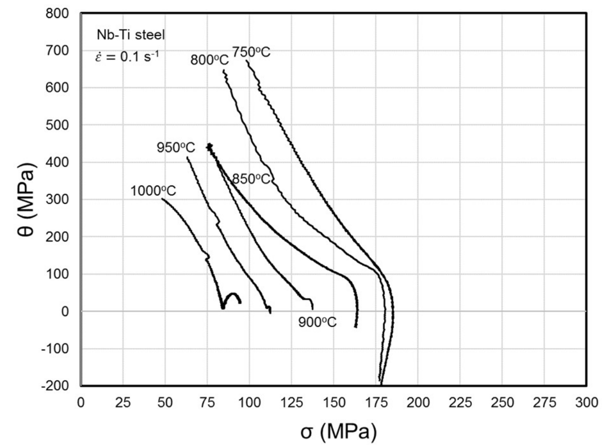

d) $\theta - \sigma$ plots for the Nb-Ti steel at 0.1 s-1

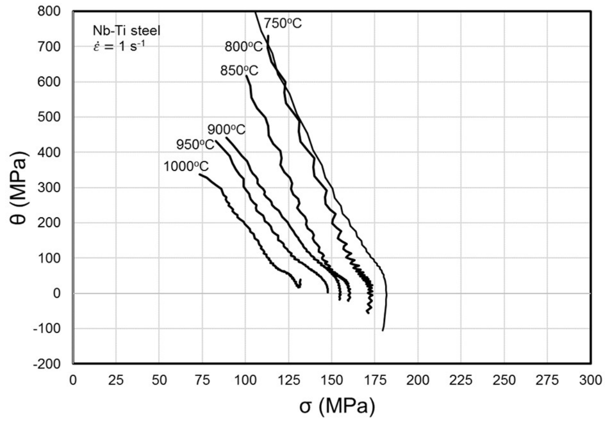

e) $\theta - \sigma$ plots for the Nb-Ti steel at 1 s-1

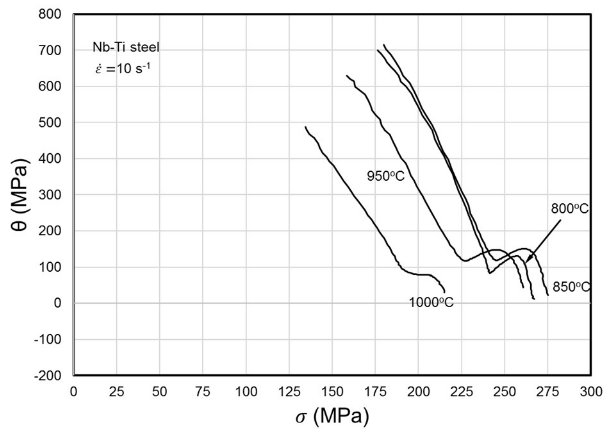

f) $\theta - \sigma$ plots for the Nb-Ti steel at 10 s-1

Figure 3 – The Kocks-Mecking plots of $\boldsymbol{\theta}$ versus $\boldsymbol{\sigma}$ for the determination of characteristic stresses: $\boldsymbol{\sigma_c}$, $\boldsymbol{\sigma_p}$, and $\boldsymbol{\sigma_{ss}}$ for temperature range 1000 to 750 °C for VN steel a) to c) and Nb-Ti d) to f) at strain rates of 0.1, 1 and 10 s^{-1}, respectively.

3.3 Estrin and Mecking approach (EM model)

An alternative approach was using $\sigma\theta - \sigma^2$ plots, to study work-hardening behaviour, **Figure 4**. The definition of the critical points on the $\sigma\theta - \sigma^2$ plots are similar to those for the $\theta - \sigma$ plots. However, the linearity of these plots form the basis of the accuracy of both the KM and EM theoretical work-hardening DRV models. Comparatively, it can be observed that the EM approach gives better linearity for both Nb-Ti and VN steels. The saturation stress σ_{sat}, recovery rate r, the softening rate s_r and curvature factor expressed by r/s_r have been given in Table II and Table III for VN steel and Nb-Ti steel, respectively.

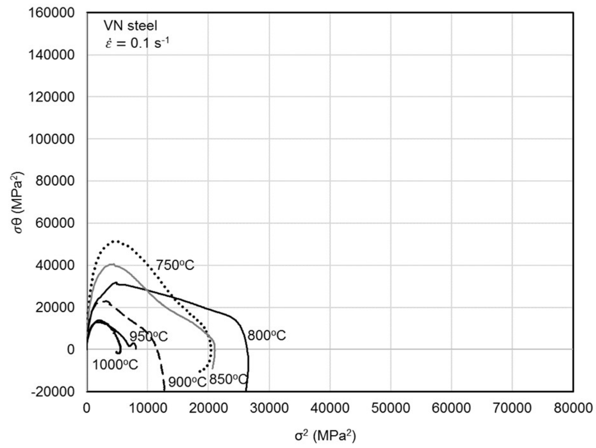

a) EM plots of $\sigma\theta - \sigma^2$ for the VN steel at 0.1 s^{-1}

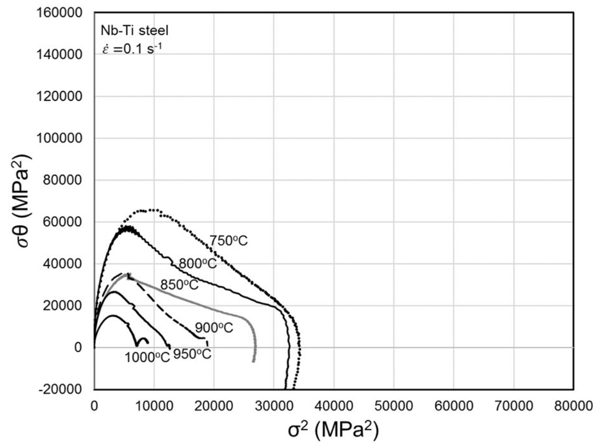

d) EM plots of $\sigma\theta - \sigma^2$ for the Nb-Ti steel at 0.1 s^{-1}

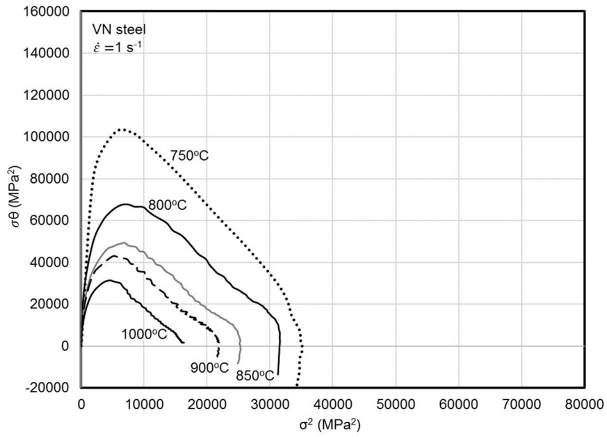

b) EM plots of $\sigma\theta - \sigma^2$ for the VN steel at 1 s^{-1}

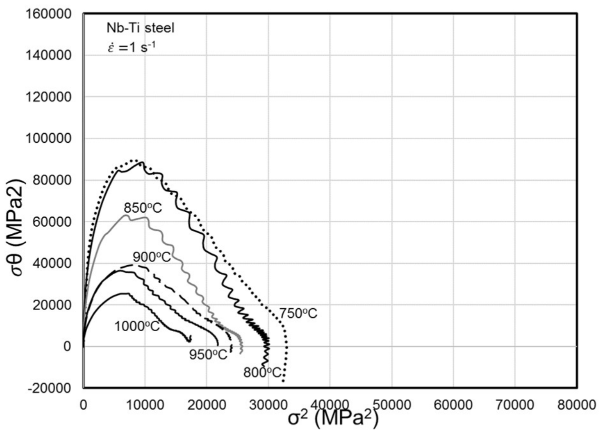

e) EM plots of $\sigma\theta - \sigma^2$ for the Nb-Ti steel at 1 s^{-1}

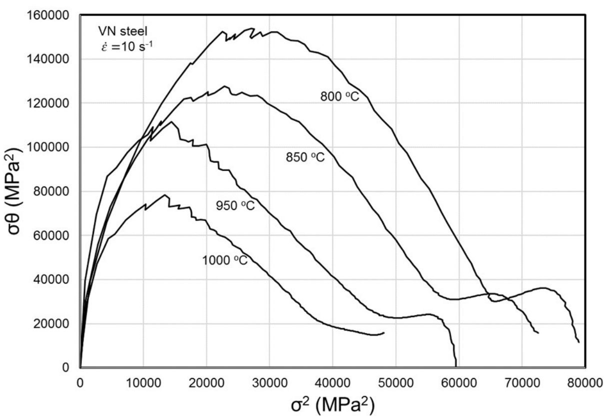

c) EM plots of $\sigma\theta - \sigma^2$ for the VN steel at 10 s^{-1}

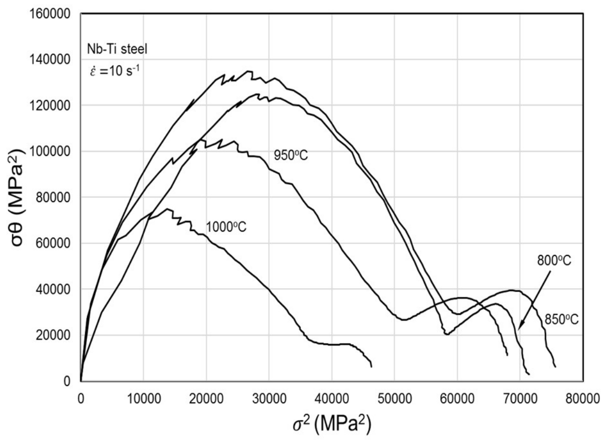

f) EM plots of $\sigma\theta - \sigma^2$ for the Nb-Ti steel at 10 s^{-1}

Figure 4 – Plots of $\boldsymbol{\sigma\theta}$ versus $\boldsymbol{\sigma^2}$ showing the interaction between work hardening and softening mechanisms (DRV, DRX and DT) derived from compression curves to determine characteristic points and recovery rates $\boldsymbol{r}$ for the hypothetical WH/DRV curve. The inflections on the linear denotes DRV and DT while deviation from linearity signified start of DRX, respectively.

Table II – The VN steel's saturation stress, recovery rate, softening rate and curvature factor obtained from Figure 4, at different temperatures and strain rates.

Temp. (°C)	Strain rate, $\dot{\varepsilon}$ (s^{-1})	Sat. stress σ_{sat} (MPa)	Flow stress $\sigma_{0.02}$ (MPa)	Strain at yield $\varepsilon_{0.02}$	Peak stress (MPa)	Peak strain	Softening rate s_r	Recovery rate r	Curvature factor, r/s_r
750	0.1	152	70	0.05	142.85	0.44	3.8	7.07	1.9
	1	203	103	0.08	187.4	0.4	6.4	None	1
800	0.1	204	72	0.06	162.65	0.55	1.8	None	(1.3)
	1	192	99	0.08	177.6	0.44	4.4	5.3	1.2
850	0.1	153	69	0.06	145.1	0.61	3.7	5.6	1.5
	1	172	83	0.06	158.9	0.52	3.7	5.2	1.4
900	0.1	117	47	0.05	-	-	4.4	None	1
	1	155	82	0.07	148.2	0.57	4.2	5.7	1.4
950	0.1	96	41	0.07	-	-	3.7	None	1
	1	117	75	0.09	-	-	4.5		3
1000	0.1	81	46	0.04	74.9	0.3	7.4	None	1
	1	130	69	0.04	-	-	5.3	7.2	1.4

Note: The curvature factor in parenthesis signifies that the value did not arise from curve fitting, and σ_0 and ε_0 are the yield stress and strain at 2% offset

Table III – Saturation stress, recovery rate, softening rate and curvature factor in the Nb-Ti steels obtained from Figure 4, at different temperatures and strain rates.

Temperature (°C)	Strain rate, $\dot{\varepsilon}$ (s^{-1})	Sat. stress σ_{sat} (MPa)	Flow stress σ_0 (MPa)	Strain at yield ε_0	Peak stress	Peak strain	Softening rate s_r	Recovery rate r	Curvature factor, r/s_r
750	0.1	200	101	0.06	185.3	0.45	4.6	None	1
	1	187	97	0.06	181.7	0.43	7.2	None	1
800	0.1	217	83	0.05	180.5	0.51	2.2	4.7	2.2 (1.4)
	1	176	113	0.07	173.6	0.5	5.5	9.7	1.8
850	0.1	203	76	0.04	164.1	0.6	1.7	2.2	1.3
	1	171	101	0.06	160.7	0.55	2.6	9.2	3.5

900	0.1	140	76	0.06	-	-	4.17	6.1	1.5
	1	164	89	0.06	155.1	0.57	3.6	4.9	1.4
950	0.1	114	62	0.05	-	-	5.8	None	1
	1	159	83	0.05	147.7	0.6	3.0	5.4	1.8
1000	0.1	91	48	0.05	-	-	7.3	None	1
	1	134	73	0.04	-	-	4.5	?	1.4

Note: The values in parenthesis were obtained as given in Table **II**.

4.0 Discussion

4.1 Dynamic recovery (DRV) in low temperature austenite

DRV occurs concurrently with work hardening (WH) during high temperature plastic deformation and is characterized by a release of stored energy without any migration or movement of high angle boundaries (HABs) [13]. The DRV process involves either annihilation of dislocations or rearrangement of dislocations (generally referred to as knitting and unravelling of dislocations) due to dislocation climb, cross-slip and glide to attain low energy through formation of low angle subgrain boundaries [13, 14, 15]. In this study, the difference between the strain at the point of yielding $\sigma_{0.02}$ and the critical strain ε_c for either DT or DRX, whichever comes first shows the extent of DRV. In agreement with other studies, DRV was present though to a lesser extent since austenite in these steels is a low stacking fault energy (SFE) material.

DRV was more pronounced when the strain rate was increased and also at intermediate temperatures where both DRX and DT were present, Figure **3** and Figure **4**. Under these conditions a peak was not attained for these tests. Contrary to most workers [9, 16] who attribute the lack of a peak in low temperature austenite to DRV-only as the restoration mechanism (i.e. DRV is sufficient to counteract the increase of flow stress caused by mechanical hardening when DRX does not occur), the coexistence of concurrent deformation, DRV, DT and DRX lead to a DRX-DT inter-mode curve (mostly referred to in the literature as a DRV type curve). For the DRX-DT intermode curves, the peak was delayed to higher strains that were not attained under the deformation conditions of this study, Figure **2**. The dominant restoration mechanism in stable austenite (low SFE), therefore, was DRX while in the case of unstable austenite (low austenite temperatures) DRV, DRX and DT were the competing restoration mechanisms with DT and DRV being favoured. At low austenite temperatures DT was dominant limiting the extent of DRV in the process. In the presence of dynamic restoration processes, Ebrahimi and Solhjoo [17] divided the flow curves into two zones, with Zone I: a WH and DRV regime (between σ_0 and σ_c) and Zone II: a WH and DT/DRX regime, between σ_c and a steady state condition. As reported by Devadas [9] for the "DRV type curve", a plateau or saturation stress is expected with increasing strain.

4.2 Theoretical DRV work-hardening models: The Kocks and Mecking and the Estrin and Mecking approaches

For high SFE materials which only dynamically recover (i.e. ferrite), the flow stress reaches a saturation steady state value at high strains. The methodologies which enable such behaviour to be modelled have been presented previously [18] and will be reviewed here in relation to a hypothetical deformation curve of VN and Nb-Ti microalloyed steels deformed at low austenite temperatures. It should also be noted that in low SFE materials as in austenite, the modelling of the hypothetical flow stress curve for WH and DRV plays a critical role in most phenomenological flow stress constitutive models, which incorporate effects of restoration kinetics on the hypothetical flow stress curve in the flow stress prediction/determination. Both the theoretical WH and DRV curves/models and flow stress models are considered as second stage constitutive equations [18]. There are two distinct approaches to describe the extrapolated flow curves based on functional dependence of the hardening coefficient on the flow stress [19]: a) the Kocks-Mecking (KM) model represented by a linear relationship in the θ vs σ coordinates, and b) the Estrin-Mecking (EM) model which proposes a hyperbolic behaviour of θ with σ and linearity is predicted by the $\sigma\theta$ vs σ^2 plot (see Appendix 1).

The KM based their approach on a thermal activation process which controls plastic deformation behaviour at strain rates below 10^3 s^{-1} [20]. Estrin and Mecking [19] developed the EM model which is an improvement on the KM model. There is unanimity that the EM approach provides a better fit compared with other models, including the MK [6, 21]. This was also verified in the linearity obtained when the two approaches were compared in Figure 3 and Figure **4**. The modified DRV model in this work was, therefore based on the EM approach.

Appendix 1 provides a detailed derivation of the EM model. The work hardening parameters r and h obtained from the $2\theta\sigma$ versus σ^2 plots can be presented as functions of the Zener-Hollomon temperature compensated strain rate Z, which represents the dependence of the saturation stress on Z [22]. The relationships are obtained from plots of $\ln r/\ln \sigma_{rec}$ versus $\ln Z$ [2]. Several authors have reported that by contrast, the value of r decreases with Z, indicating that dynamic recovery becomes less effective as the temperature is decreased or the strain rate is increased [2, 22]. Quelennec and Jonas [22] further suggested that the r value appears to saturate at high Z values and can, therefore, be consider as a constant under such conditions.

4.3 The modified DRV work-hardening model

In agreement with the literature [6], it was observed that at high temperatures where DRX was dominant the EM model (as described in 4.2) proved an accurate representation of the stress–strain behaviour in the work-hardening regime, Figure 8. Additionally, it was observed through this work that, at low temperatures where DT was the only softening mechanism, the original EM model provided the best fit, Figure 7. At intermediate temperatures between 800 and 950 ^{o}C, however, the EM model's stress predictions deviated from the measured values, Figure 6. An improved EM model with an additional parameter was derived to provide consistency with experimental data, Figure 6.

Figure 5 compares the original and modified EM models, clearly showing an improvement in the in the unstable austenite temperature range. The modified DRV WH model also accounts for the fractional softening after the critical strain for DT which is central in phenomenological/mathematical flow stress models.

At low temperatures, where DT is the only softening mechanism and at high temperatures where DRX is dominant, the work-hardening stress-strain curve obeys the original EM model given by (see Appendix 1 – Derivation of the Estrin and Mecking work hardening model):

$$\sigma = \left[\sigma_{sat}^2 - (\sigma_{sat}^2 - \sigma_0^2)\exp\left(-s_r(\varepsilon - \varepsilon_0)\right)\right]^{1/2} \qquad \text{Equation 1}$$

The DT/DRX inter-mode region was observed at intermediate temperatures and/or at higher strain rates where restoration was mainly by recovery, DT and DRX. The flow behaviour obeyed the following modified DRV work-hardening model for the inter-mode region:

$$\sigma = \left[\sigma_{sat}^2 - (\sigma_{sat}^2 - \sigma_0^2)\exp\left(-\left(\frac{r}{s_r}\right)(\varepsilon - \varepsilon_0)\right)\right]^{1/2} \qquad \text{Equation 2}$$

where the softening rate s_r and the newly defined parameters: recovery rate r and curvature factor (r/s_r), are given in Table II and Table III for VN and Nb-Ti steels.

From Table **II** and Table **III** for the VN and Nb-Ti steels respectively, the recovery rate r was determined to be constant in the DT/DRX inter-mode region and lower than when DRX or DT is dominant. For temperatures where DT-only or DRX is dominant, the recovery rate r was found to be comparable, i.e. ~5.4 for VN steels. Increase in strain rate shifts the DT/DRX region to higher temperatures. This can be observed in the r for the Nb-Ti which had higher Ar_3 temperatures and deformation was mostly in the DT dominant regime.

The curvature factor describes the predicted or hypothetical work-hardening stress curve when work-hardening is counteracted by DRV, DT and DRX. In this case, the parameter $\frac{r}{s_r} \sim 1.2 \pm 0.9$ for the VN steel while $\frac{r}{s_r} \sim$ 1.5±0.7 for the Nb-Ti steel. This indicated that Nb-Ti steels recovered more readily and softening was delayed compared to the VN steels at the same temperature. The finding is also supported by the critical transformation temperatures which were comparatively higher in Nb-Ti steel than in the VN steel, see Ref. [7]. High transformation temperatures also dictated the existence of Dynamic Transformation or DT at considerably elevated temperatures above the Ar_3 temperature.

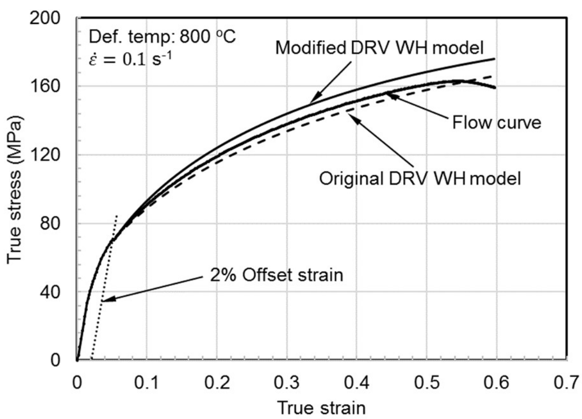

a) Work-hardening flow curves for the VN steel

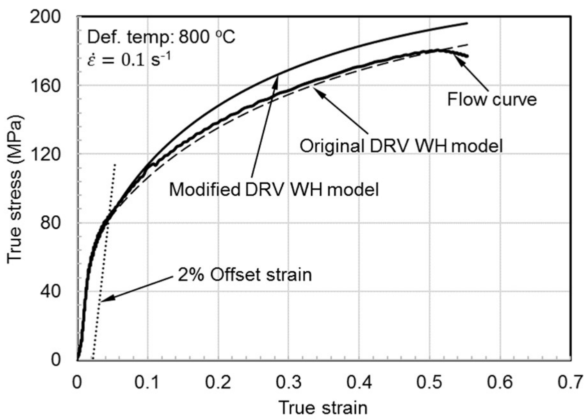

b) Work-hardening flow curves for the Nb-Ti steel

Figure 5 – Comparison between the original EM model's curve and the modified DRV work-hardening model, indicating softening after the critical strain for dynamic transformation, $\varepsilon_{c\ DT}$

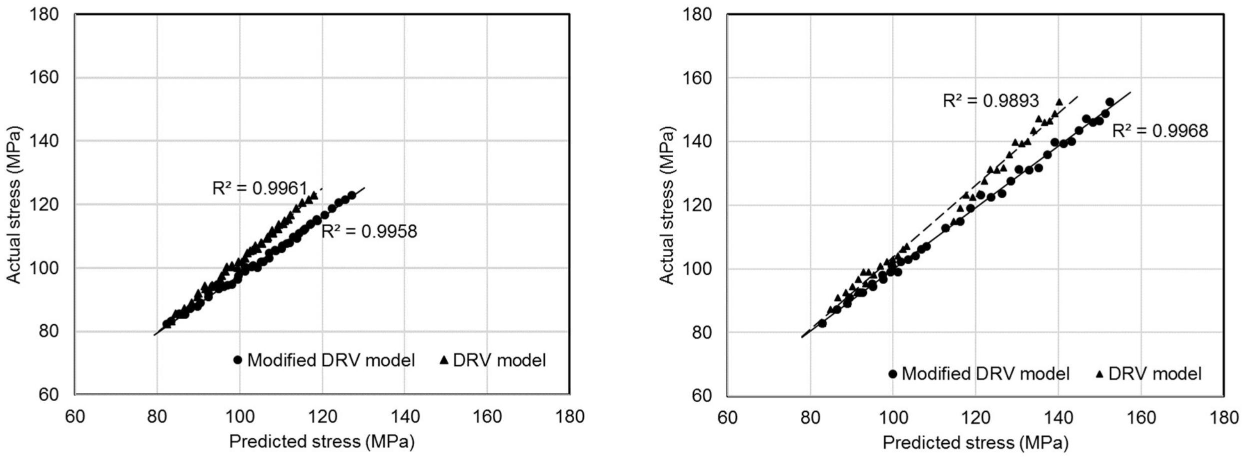

a) The VN steel

b) The Nb-Ti steel

Figure 6 – The Actual (measured) stress versus predicted stress plot for the modified DRV model and the original EM DRV work-hardening models for a) the VN steel and b) the Nb-Ti steel in the inter-mode DT/DRX region at temperatures between 800 and 950 °C and at a strain rate of 1 s^{-1}

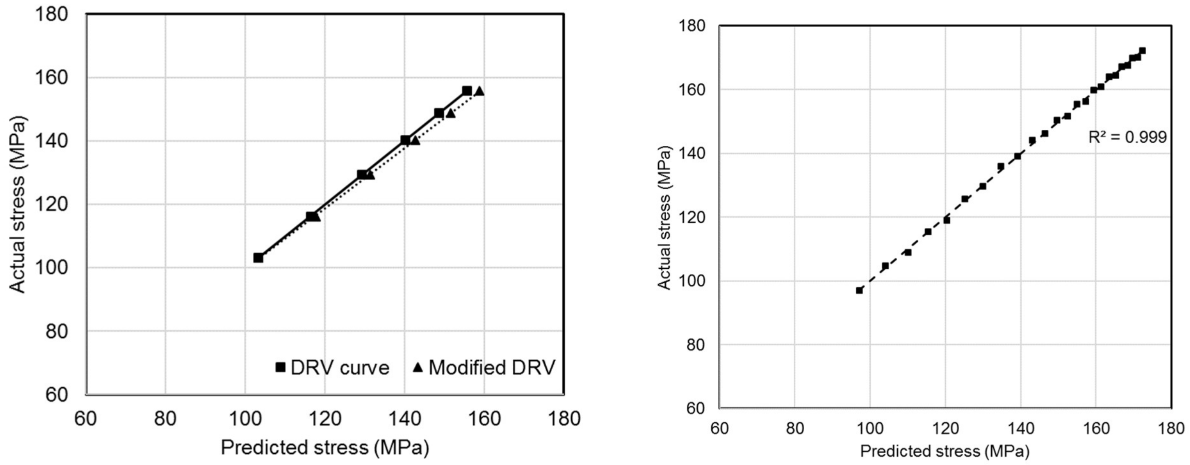

b) The Nb-Ti steel

a) The VN steel

Figure 7 – The Actual stress versus predicted stress plot for the original EM DRV work-hardening models in the DT-dominant region at a strain rate of 1 s^{-1} and a temperature of 750 ^oC for a) the VN steel and b) the Nb-Ti steel

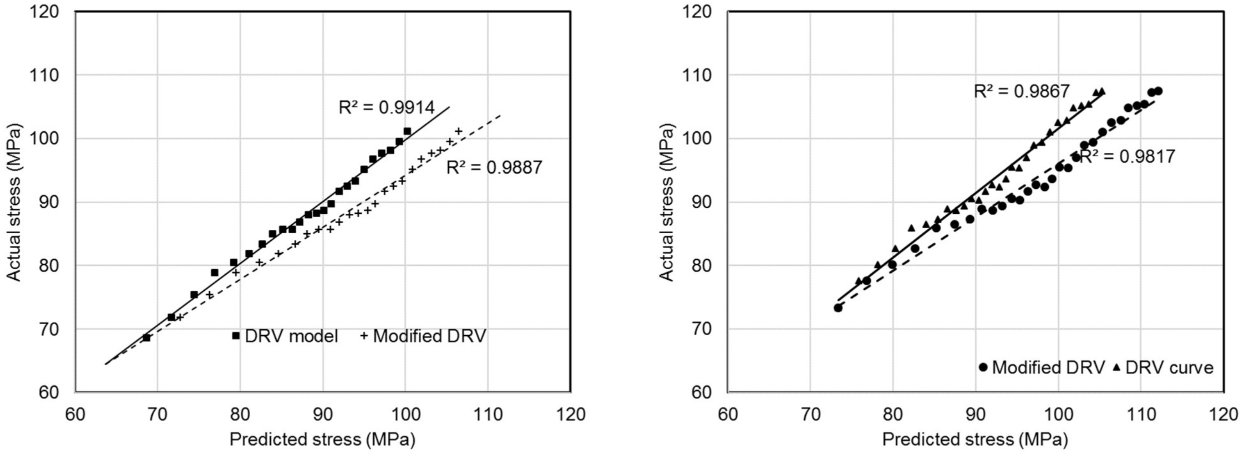

a) The VN steel

b) The Nb-Ti steel

Figure 8 – The Actual stress versus predicted stress plot for the modified DRV model and the original EM DRV work-hardening models in the DRX-dominant region at a strain rate of 1 s^{-1} and at a temperature of 1000 ^oC for a) the VN steel and b) the Nb-Ti steel

5.0 Conclusion

1. A computational modified DRV work-hardening model based on the Estrin and Mecking approach and applicable to the unstable austenite region, has been developed.
2. The effect of both the recovery rate parameter r and the softening rate parameter s_r on work-hardening has been considered. The model provided

good correlation between measured and predicted stresses in the range between the flow stress and critical stress at deformation in the low austenite temperature region.

3. When extrapolated, the modified DRV model was also able to reveal softening after the critical strain for dynamic transformation making this model more applicable in the determination of fractional softening, X in the phenomenological modelling of the mean flow stress in hot rolling.

Acknowledgements
This work has been performed with funding from the University of Pretoria and technical support from the Industrial Minerals and Metals Research Institute (IMMRI). Generous help from Rorisang Maubane is gratefully acknowledged for providing on-equipment training and technical support on the Bähr 850AD™ and Gleeble 1500™ during tests.

References

[1] O. Bouaziz, "Revisited Storage and Dynamic Recovery of Dislocation Density Evolution Law: Toward a Generalized Kocks-Mecking Model of Strain-Hardening," *Advanced Engineering Materials,* vol. 14, no. 9, pp. 759-761, 2012.

[2] A. Momeni, S. M. Abbasi and H. Badri, "Hot deformation bahaviour and constitutive modelling of VCN 200 low alloy steel," *Applied Mathematical Modelling,* vol. 36, pp. 5624-5632, 2012.

[3] M. Meysami and S. A. A. A. Mousavi, "Study on behaviour of medium carbon vanadium microalloyed steel by hot compression test," *Materials Science and Engineering A,* vol. 528, pp. 3049-3055, 2011.

[4] H.-l. Wei, G.-q. Liu, X. Xiao and M.-h. Zhang, "Dynamic recrystallization behavior of a medium carbon vanadium microalloyed steel," *Materials Science and Engineering A,* vol. 573, pp. 215-221, 2013.

[5] H. Mirzadeh, J. M. Cabrera, J. M. Prado and A. Najafizadeh, "Hot deformation behaviour of a medium carbon microalloyed steel," *Materials Science and Engineering A,* vol. 528, pp. 3876-3882, 2011.

[6] P. D. Hodgson, L. X. Kong and C. H. J. Davies, "The prediction of the hot strength in steels with an integrated phenomenological and artificial neural network model," *Journal of Materials Processing Technology,* vol. 87, pp. 131-138, 1999.

[7] S. A. J. Chalimba, R. J. Mostert, W. Stumpf, K. M. Banks and C. W. Siyasiya, "Effects of roughing on finish rolling simulations in microalloyed strip steels," *Accepted for publication,* 2016.

[8] B. Roebuck, J. D. Lord, M. Brooks, M. S. Loveday, C. M. Sellars and R. W. Evans, Measurement Good Practice Guide No 3 - Measuring Flow Stress in Hot Axisymmetric Compression Tests, United Kingdom: National Physical Laboratory, 2002.

[9] C. Devadas, D. Baragar, G. Ruddle and I. V. Samarasekera, "The Thermal and Metallurgical State of Steel of Steel Strip during Hot Rolling: Part II. Factors Influencing Rolling Loads," *Metallurgical Transactions A,* vol. 22A, pp. 321-333, 1991.

[10] Dynamic Systems Inc, Gleeble Systems Application Note: Flow Stress Correction in Uniaxial Compression Testing, New York: DSI, 2003.

[11] J. J. Jonas, X. Quelennec, L. Jiang and E. Martin, "The Avrami kinetics of dynamic recrystallization," *Acta Materialia,* vol. 57, pp. 2748-2756, 2009.

[12] P. D. Hodgson, J. J. Jonas and C. H. J. Davies, "Modeling of hot and warm working of steels," in *Handbook of thermal process modeling of steels Thermal Process Modelling of Steels*, New York, CRC Press, 2008, pp. 225-65.

[13] R. D. Doherty, D. A. Hughes, F. J. Humphreys, J. J. Jonas, D. J. Jensen, M. E. Kassner, W. E. King, T. R. McNelley, H. J. McQueen and A. D. Rollett, "Current issues in recrystallization: a review," *Materials Science and Engineering A,* vol. 238, pp. 219-274, 1997.

[14] C. Roucoules, "Dynamic and Metadynamic Recrystallization in HSLA Steels," PHD Thesis, McGill University, 1992.

[15] R. Ebrahimi and E. Shafiei, "Mathematical Modeling of Single Peak Dynamic Recrystallization Flow stress curves in Metallic alloys," 2012. [Online]. Available: http://www.intechopen.com/books/recystallization/mathematical-modelling-of-sinlge-peak-dynamic-recrystallization-flow-stress-curves-in-metallic-alloys. [Accessed 30 May 2015].

[16] R. H. Wu, J. T. Liu, H. B. Chang, T. Y. Hsu and X. Y. Ruan, "Prediction of the flow stress of 0.4C-1.9Cr-1.5Mn-1.0Ni-0.2Mo steel during hot deformation," *Journal of Materials Processing Technology,* vol. 116, pp. 211-218, 2001.

[17] R. Ebrahimi and S. Solhjoo, "Characteristic Points of Stress-Strain Curve at High Temperature," *International Journal of ISSI,* vol. 4, no. 1,2, pp. 24-27, 2007.

[18] S. B. Davenport, N. J. Silk, C. N. Sparks and C. M. Sellars, "Development of constitutive equations for modelling of hot rolling," *Materials Science and Technology,* vol. 16, pp. 539-547, 2000.

[19] Y. Estrin and H. Mecking, "A unified phenomenological description of work hardening and creep based on one-parameter models," *Acta Metall.,* vol. 32, no. 1, pp. 57-70, 1984.

[20] N. Tsuchida, Y. Izaki, T. Tanaka and K. Fukaura, "Effects of Temperature and Strain Rate on STress-Strain Curves for Dual-Phase Steels and Their Calculations by Using the Kocks-Mecking Model," *ISIJ International,* vol. 52, no. 4, pp. 729-734, 2012.

[21] L. X. Kong, P. D. Hodgson and D. C. Collinson, "Extrapolative prediction of the hot strength of austenitic steels with a combined constitutive and ANN model," *Journal of Materials Processing Technology,* vol. 102, pp. 84-89, 2000.

[22] X. Quelennec and J. J. Jonas, "Simulation of Austenite Flow Curves under Industrial Rolling Conditions Using a Physical Dynamic Recrystallization Model," *ISIJ International,* vol. 52, no. 6, pp. 1145-1152, 2012.

Appendix 1 – Derivation of the Estrin and Mecking work hardening model

Estrin and Mecking [19] modelled the flow curves up to the peak stress based on the evolution of dislocation density from concurrent work hardening and dynamic recovery (DRV) only. In this approach, the evolution of dislocation density with strain was determined as the sum of differential hardening and softening terms as follows [2, 19]:

$$\frac{d\rho}{d\varepsilon} = \left(\frac{d\rho}{d\varepsilon}\right)^{+} + \left(\frac{d\rho}{d\varepsilon}\right)^{-}$$

Where the first term represents the work hardening part and the second term the softening due to DRV. The terms in the equation above for dependence of the dislocation density ρ on plastic strain ε can be replaced as follows [19]:

$$\frac{d\rho}{d\varepsilon} = h - r\rho$$

Where h is the athermal work-hardening rate ($h = r\frac{\sigma_{sat}^2}{(\alpha\mu b)^2}$) and r denotes the rate of dynamic recovery at a given temperature and strain rate, independent of the strain.

$d\varepsilon$ can be expressed as: $d\varepsilon = \frac{d\rho}{h-r\rho}$

and $d\rho$ in turn, can be defined as: $d\rho = \frac{d(h-r\rho)}{-r}$

Combining the two equations above leads to: $-rd\varepsilon = \frac{d(h-r\rho)}{h-r\rho}$

the integration of which gives: $\ln(h - r\rho) = -r\varepsilon + C$

The exponential of the above relationship and making dislocation density ρ the subject:

$$\rho = \frac{h - \exp(-r\varepsilon + C\varepsilon)}{r} = \frac{h}{r} = \frac{C_1}{r}\exp(-r\varepsilon)$$

By employing the limiting condition $\varepsilon = 0$ and $\rho = \rho_0$ (the value at yielding), that of C_1 can be derived as $h - r\rho_0$. This leads to the expression:

$$\rho = \frac{h}{r} - \frac{(h - \rho_0 r)}{r}\exp(-r\varepsilon)$$

or

$$\rho = \rho_0\exp(-r\varepsilon) + \frac{h}{r}[1 - \exp(-r\varepsilon)]$$

The dislocation density ρ is converted into σ using the expression $\sigma = M\alpha G_M b\sqrt{\rho}$ so that ρ and ρ_0 can be replaced by $(\sigma/MG_M b)^2$ and $(\sigma_0/MG_M b)^2$, respectively. Under these conditions, the flow stress can be given by the following relationship in terms of the plastic strain:

$$\sigma = \left[\sigma_0^2 \exp(-r\varepsilon) + (M\alpha G_M b)^2 \frac{h}{r}(1 - \exp(-r\varepsilon))\right]^{1/2}$$

where σ_0 and σ_{sat} denote the yield (initial) and saturated stress defined as $(\alpha M G_M b)^2 \rho_0$ and $(\alpha M G_M b)^2 (h/r)$, respectively, α is a shape factor in the order of unity, M is the Taylor factor (3.07 for FCC materials), G_M is the shear modulus, b is the magnitude of Burger's vector (b was evaluated to be 0.2594 nm for a carbon content of 0.07% and at 1000 °C [11]) and ρ_0 is the initial dislocation density.

When ε tends to infinity, the above equation can be rewritten as follows:

$$\sigma \approx M\alpha G_M b \sqrt{\frac{h}{r}}$$

The expression $M\alpha G_M b\sqrt{\frac{h}{r}}$ can be defined as the dynamic recovery saturation stress, σ_{sat} which allows the work hardening stress curve to be written in the following formalization [11, 22]:

$$\sigma = \left[\sigma_{sat}^2 - (\sigma_{sat}^2 - \sigma_0^2)\exp\big(-r(\varepsilon - \varepsilon_0)\big)\right]^{1/2}$$

Further simplification is achieved by the assumption that $\rho_0 \approx 0$ when compared to the stored dislocation density during hot deformation. An assumption is also that it is more pertinent to a low SFE material such as austenite characterized by a sluggish DRV. Neglecting ε_0 in this case, yields the following expression for the flow curve:

$$(\sigma_{sat}^2 - \sigma_0^2)\exp(-r\varepsilon) = \sigma_{sat}^2 - \sigma^2$$

Considering the plastic flow curve only after yielding (i.e. $\sigma_0 = 0$), the simplified work hardening curve, therefore, can be rewritten as follows:

$$\sigma = \sigma_{sat}(1 - \exp(-r\varepsilon))^{0.5}$$

The differentiation of which gives:

$$\frac{d\sigma}{d\varepsilon} = 0.5\sigma_{sat} r \exp(-r\varepsilon)\,(1 - \exp(-r\varepsilon))^{-0.5}$$

Substituting $1 - (\sigma/\sigma_{sat})^2$ for $\exp(-r\varepsilon)$, the differential equation can be written as:

$$\theta = \frac{d\sigma}{d\varepsilon} = 0.5r\left(\frac{\sigma_{sat}^2 - \sigma^2}{\sigma}\right) \quad \text{or} \quad \sigma\theta = \sigma\frac{d\sigma}{d\varepsilon} = 0.5r(\sigma_{sat}^2 - \sigma^2)$$

From the above expression, the plots of $\sigma\theta$ versus σ^2 are linearly fitted from which the slope m and the abscissa and intercept are $-0.5r$ and $-0.5r\sigma_{sat}^2$, respectively. Thus r is the value of the recovery parameter which specifies the "curvature" of the dynamic recovery curve [11].